

Probing the Local Dynamics of Nucleotide-Binding Pocket Coupled to the Global Dynamics: Myosin versus Kinesin

Wenjun Zheng and Bernard R. Brooks

Laboratory of Computational Biology, National Heart, Lung, and Blood Institute, National Institutes of Health, Bethesda, Maryland

ABSTRACT Based on the elastic network model, we develop a new analysis for protein complexes, which probes the local dynamics of a subsystem that is elastically coupled to a fluctuating environment. This method is applied to a comparative dynamical analysis of the nucleotide-binding pocket of two motor proteins—myosins and kinesins. In myosins, the observed structural changes in the nucleotide-pocket from the transition state to the rigorlike state are dominated by the lowest normal mode that involves significant movements in both switch I and switch II; in kinesins, the measured conformational changes in the nucleotide-pocket are also dominated by the lowest mode, which, however, only involves large movement in switch I. We then compute the global structural changes induced by the nucleotide-pocket deformations as described by the dominant pocket-mode, which yield encouraging results: in myosins, multiple hinge motions involving the opening/closing of the cleft between the upper and lower 50 -kDa subdomains and the swinging movement of the converter are induced, which are dominated by precisely the same global mode that has been recently identified by us as important to the dynamical correlations among the nucleotide-pocket, the actin-binding site, and the converter; in kinesins, the induced global conformational changes are well described by a highly collective global mode which hints for a dynamical pathway spanning from the nucleotide-pocket to the neck-linker via the H6 helix.

INTRODUCTION

Motor proteins are specialized ATPases that transport cargo by coordinating the ATP hydrolysis with binding to and movement along a filament. They are believed to be capable of sensing and responding to the presence or absence of a γ -phosphate and transmitting this information along a pathway of increasingly larger conformational changes that ultimately results in a force-generating event (1). The detailed mechanism of force-generation has been actively investigated (1–3).

The two best-studied motor proteins, myosin and kinesin, are dimeric proteins that contain a central core of structural elements that are remarkably similar (4). Despite this structural homology, the kinesin motors differ substantially from the myosins in their mechanism. A major difference is the nucleotide-dependent interactions of the motors with their filament (actin for myosins, microtubule for kinesins): myosin bound to ATP is weakly bound to or detached from actin, whereas kinesin-ATP is strongly bound to microtubules. Conversely, myosin-ADP is strongly bound to actin, whereas kinesin-ADP is weakly bound to or detached from microtubules. For both motors, the rate-limiting step in the ATPase cycle is accelerated by its binding to its filament, which results in a characteristic actin- or microtubule-activated ATPase activity: whereas binding of actin causes myosin to release products, the binding of microtubules enables hydrolysis in kinesin (1).

For myosins, the available crystal structures and cryo-EM results capture their conformations in several structural states with no nucleotide, a transition state analog, or MgADP

bound to the nucleotide-pocket. These states include: transition state; near-rigor state; detached state (5); and rigorlike state (6–9). The transition state mimics the pre-power-stroke state compatible with ATP hydrolysis and before actin binding. The near-rigor state was initially proposed to reveal the position of the lever arm at the end of the power stroke on release of MgADP; however, kinetic evidence showed that it cannot bind strongly to actin without significant structural rearrangements (3). So it is now believed to be a weak-binding state that occurs shortly after detaching from actin. The detached state is argued to be a stable ATP state with unwound SH1 helix and unconstrained converter/lever arm (5). The newly solved crystal structures of rigorlike state (6,7) appear to resemble the strong-binding state that occurs at the end of a power-stroke.

For kinesins, the structural states have not been clearly defined by the available structures. Almost all the solved crystal structures are ADP-bound (except for a KIF1A structure 1I6I). Although the comparison of these structures only revealed relatively small differences (10), it helps to identify the mechanical elements that undergo conformational changes during the ATPase cycle. The ADP-state is believed to be a weak-binding state. The strong-binding ATP state still eludes crystallographers and may need the binding of microtubules to stabilize it.

The nucleotide-binding pocket of both myosins and kinesins is comprised of four conserved pieces: N₁ (P loop); N₂ (switch I); N₃ (switch II); and N₄ (base). These regions are strongly conserved between myosins and kinesins. However, the environment of their pocket is very different: in kinesins it is exposed on the surface of the protein rather than enclosed between two subdomains of the

Submitted March 22, 2005, and accepted for publication April 25, 2005.

Address reprint requests to W. Zheng, Tel.: 301-451-2014; E-mail: zhengwj@helix.nih.gov.

© 2005 by the Biophysical Society

0006-3495/05/07/167/12 \$2.00

doi: 10.1529/biophysj.105.063305

protein as in myosins. The switches I and II are γ -phosphate sensors that engage with phosphate through hydrogen bonding on ATP binding, but disengage on phosphate release. They are believed to be critical for transmitting the pocket structural changes to remote sites of motor proteins and trigger directed movements. In myosins, a salt bridge between the conserved arginine of switch I and the conserved glutamic acid of switch II is believed to stabilize the closed conformation of myosin motors and to be essential for nucleotide hydrolysis (2). Such a salt bridge is also seen in some kinesin structures. Yun and co-workers (11) proposed that it is required for activation of the kinesin motors by the binding of microtubules.

The conformational changes in the nucleotide-pocket are observed to be significantly correlated with the global conformational changes that are responsible for actin/microtubules binding and ultimately the motor movement: for myosins, the switch I's opening/closing is associated with the closing/opening of the actin-binding site (6,8), and the switch II's opening/closing is associated with the downward/upward swinging of the lever arm (2). For kinesins, a closed pocket (ATP-bound) is associated with the strong-binding mode of the microtubule-binding site and the neck-linker being docked to the core domain (1). Therefore, a detailed comparison of the local dynamics of the nucleotide-binding pocket between myosins and kinesins may reveal their differences in the global dynamics that could hint for different force-generation mechanisms. Such a comparative study is feasible because of the following reasons: first, the nucleotide-binding pocket is highly homologous between myosins and kinesins, so a residue-to-residue comparison is possible (this is not possible for the whole motor domain which lacks such homology); and second, the small size of the pocket (24 residues) as compared with the large size of the whole motor domain makes the analysis computationally inexpensive, given that the effective interactions of coupling between the nucleotide-pocket and the rest of the motor domain are modeled properly.

Modeling the dynamics of motor proteins has been done at a variety of resolution levels ranging from all-atom simulations (12,13) to identification of rigid-body motions of subunits during the hydrolysis cycle (14). Full-scale molecular dynamics studies of motor proteins with all atom details are still limited both by size and by timescale. The characterization of observed structural changes in terms of rigid-body motions of subunits, while being intuitively appealing, is limited by the availability and relevance of crystal structures.

The normal-modes analysis (NMA) of a highly simplified elastic network model (ENM) has been successfully applied to the analysis of large-scale protein conformational changes in several studies (15–17). It has been recently applied to the study of motor proteins (18–21). In a recent work by one of us, the ENM is used to explore the global conformational changes induced by deforming the nucleotide-binding pocket in several motor proteins, and interesting differences were found between kinesins and myosins in terms of the

number of normal modes needed for describing the measured conformational changes (18). Motivated by these preliminary results, we further expand and test this idea in this work.

The ENM assumes elastic couplings between the nucleotide-pocket and the remaining parts of the motor domain (as environment), and the impact of such elastic couplings on the local dynamics of the pocket can be quantitatively analyzed by effectively integrating out the environment degrees of freedom (see Materials and Methods). The remaining pocket degrees of freedom are coupled by quadratic interactions that include both direct elastic interactions and indirect interactions via their couplings with the environment. The NMA of this subsystem yields various modes of movements to describe the local dynamics of the pocket, which can be validated by comparing with crystallographic data. Furthermore, given the pocket structural change described by each pocket-mode, we can analyze the global dynamics coupled to it by calculating the global conformational changes it induces (18), which helps to identify plausible dynamical pathways that transmit the pocket deformations to the remote parts of the motor domain.

MATERIALS AND METHODS

Elastic network model

Given the C_α atomic coordinates for a protein's native structure, we build an elastic network model by using a harmonic potential with a single force constant C to account for pairwise interactions between all C_α atoms that are within a cutoff distance ($R_C = 10 \text{ \AA}$). The energy in the elastic network representation of a protein is

$$E_{\text{network}} = \frac{1}{2} \sum_{d_{ij}^0 < R_C} C(d_{ij} - d_{ij}^0)^2, \quad (1)$$

where d_{ij} is the distance between the dynamical coordinates of the C_α atoms i and j , and d_{ij}^0 is the distance between C_α atoms i and j , as given in the crystal structure.

For the harmonic Hamiltonian in Eq. 1, we perform the standard normal-modes analysis (NMA). After excluding the six zero-modes corresponding to three translations and three rotations, the non-zero modes start from #1; and the mode number increases as the mode's eigenvalue increases. The eigenvectors of the lowest frequency normal modes are used to interpret the protein conformational observed crystallographically (18). The drastic simplification of representing the complex protein structure by an effective harmonic potential is justified by a study by Tirion (22) who showed that the use of a single spring constant reproduces the slow dynamics computed from the normal modes analysis of all-atom potentials. Hinsen further simplified the elastic network model to the C_α only representation (23).

Normal mode analysis (NMA) of a subsystem coupled to a flexible environment

The whole protein complex, modeled as a C_α -only elastic network, is divided into two components: the subsystem, which consists of residues (C_α s) directly involved in the functionality (for example, catalytic activity or ligand binding); and the environment, which consists of the remaining residues. We wish to study the impact of the elastic couplings between the above two components on the local dynamics of the subsystem.

Suppose the elastic energy of the whole ENM is given as follows:

$$E = xHx = x_s H_{ss} x_s + x_s H_{se} x_e + x_e H_{es} x_s + x_e H_{ee} x_e, \quad (2)$$

where $H = \begin{Bmatrix} H_{ss} & H_{se} \\ H_{es} & H_{ee} \end{Bmatrix}$ stands for the Hessian matrix of the ENM, which consists of four submatrices (H_{ss} , H_{se} , H_{es} , H_{ee}) (s , subsystem; e , environment); x_s (x_e) is the displacement vector for the subsystem (environment).

To integrate out the environment degrees of freedom, we set the gradient $\nabla_{x_e} E = 0$, which gives

$$x_e = -H_{ee}^{-1} H_{es} x_s. \quad (3)$$

Therefore

$$E = x_s H_{ss}^{\text{eff}} x_s = x_s (H_{ss} - H_{se} H_{ee}^{-1} H_{es}) x_s. \quad (4)$$

Physically, it is assumed that the environment can respond to the structural changes in the subsystem by minimizing the total energy. We note that the idea of partitioning the Hessian matrix into relevant and irrelevant parts through the use of an appropriate unitary transformation was discussed before by one of us (24).

For comparison, we can turn off the couplings, and the elastic energy of the isolated subsystem becomes

$$E = x_s H_{ss}^* x_s, \quad (5)$$

where H_{ss}^* has the same off-diagonal matrix elements as H_{ss} , but its diagonal elements are given by requiring the sum of each row/column to be zero.

Standard NMA can be performed for the harmonic subsystem described by Eq. 4. The eigenvectors of the low-frequency modes (excluding the six zero-modes) can be compared with the crystallographically measured conformational changes of the subsystem to assess their relevance to the observed structural changes.

We can also compute the global conformational changes induced by the local structural changes in the subsystem as given in Eq. 3, which establishes an important link between the local dynamics of the subsystem and global dynamics of the whole protein complex. This allows us to probe the dynamical pathway by which global conformational changes are triggered by local deformations of the subsystem.

Application to the nucleotide-pocket of myosins and kinesins

Here we define the subsystem as the nucleotide-binding pocket (consisting of four pieces: N_1 - N_4). It is highly homologous among all myosins and kinesins, so it can be structurally aligned among different kinesins and myosins. The subsystem NMA can probe the local dynamics of the nucleotide-pocket elastically coupled to the remaining parts of the motor proteins, and thereby the global dynamics coupled with the local dynamics.

Calculation of root-mean-square fluctuation (RMSF)

Based on the NMA of the ENM we can compute the root-mean-square fluctuation (RMSF) at position i (the C_α position of residue i) as

$$f_i = \sqrt{\langle \delta r_i^2 \rangle} \propto \sqrt{\sum_{m,a=x,y,z} \frac{v_{m,ia}^2}{\lambda_m}}, \quad (6)$$

where λ_m and v_m are the eigenvalue and the eigenvector of mode m solved from the NMA of H_{ss}^{eff} as described in Eq. 4. The six zero-modes are excluded. For simplification in notation, a uniform factor of T/C is omitted in Eq. 6 (T is the temperature, C is the force constant in Eq. 1).

We use Eq. 6 to compute the RMSF per residue for the nucleotide-pocket. For comparison with the RMSF results, we structurally align (with minimal

coordinate root-mean-square deviation, i.e., RMSD) the pocket conformation of every myosin/kinesin structure with the pocket conformation of a chosen reference structure by rotations and translations.

Comparison of normal modes with measured structural changes at the nucleotide-pocket

Given a reference structure of the nucleotide-pocket and the pocket-modes, we can project the measured pocket structural changes to individual modes to find the relevant mode with significant overlap (defined as the generalized cosine between the mode's eigenvector and the measured structural displacement; see Ref. 18). This serves as a mode-specific test of the quality of subsystem NMA in describing the measured structural changes (in both amplitude and direction).

Principal components analysis (PCA)

For a given reference pocket structure and a set of pocket structures, we do principal component analysis (quasi-harmonic analysis, see Ref. 25) to find the directions in configuration space that best describe the dominant structural displacements observed among the nucleotide-pocket structures. It consists of diagonalization of the covariance matrix of C_α fluctuations, after removal of overall translation and rotation. Resulting eigenvectors are directions in configuration space that represent collective motions. Corresponding eigenvalues define the mean square fluctuation of the motion along these vectors. We will keep the top two eigenvectors (P_1 and P_2), which capture the two most dominant structural displacements of the nucleotide-binding pocket.

Then we cluster all pocket conformations in a two-dimensional plot, where the two-dimensional coordinate consists of the projection coefficients obtained by projecting the structural changes from the reference pocket structure to P_1 and P_2 .

Finally we calculate the overlap (see Ref. 18) of P_1 and P_2 with each pocket-mode to test how good a single mode describes them.

Dynamical domains partition

We use a computational tool DynDom developed by Hayward (26) for dynamical domains analysis to analyze the interdomain conformational changes described by each global mode (it is downloadable from: <http://www.sys.uea.ac.uk/~sjh/DynDom/dyndom.home.html>).

Crystal structures of myosins and kinesins

The information of the crystal structures studied in this work is summarized in Table 1.

RESULTS AND DISCUSSION

We will start with the analysis of myosins' nucleotide-pocket dynamics and the global dynamics it is coupled to, which is followed by the same analysis for kinesins accompanied by a detailed comparison between them.

Myosin's nucleotide-pocket dynamics

Principal components analysis of nucleotide-pocket conformations from crystal structures

We start with a principal components analysis (PCA) of all the nucleotide-pocket conformations from myosin crystal

TABLE 1 Information of crystal structures for myosins and kinesins

Name	Source	PDB code (state or ligand)
KIF1A	<i>Mus musculus</i>	1VFZ(ADP-MG-VO4), 1VFX (ADP-MG-ALFX), 1I5S(MG-ADP), 1I6I(MG-AMPPCP)
Ncd	<i>Drosophila melanogaster</i>	2NCD, 1CZ7(dimer)
Ubiquitous Kinesin	<i>Homo sapiens</i>	1BG2, 1MKJ
Kinesin Kar3	<i>Rattus norvegicus</i> <i>Saccharomyces cerevisiae</i>	2KIN, 3KIN 3KAR, and its mutants: 1F9U, 1F9T
Fast Kinesin	<i>Neurospora crassa</i>	1GOJ
Eg5	<i>Homo sapiens</i>	1II6
Internal Kinesin	<i>Plasmodium falciparum</i>	1RY6
Myosin II	<i>Dictyostelium discoideum</i>	1MMA(N), 1VOM(T), 1Q5G(R); 1FMW(N), 1FMV(N), 1LVK(N), 1MMG(N), 1MMN(N), 1MMD(N), 1MND(T), 1MNE(N)
Scallop Myosin II	<i>Argopecten irradians</i>	1SR6, 1S5G, 1QVI and 1DFL(T), 1B7T and 1KK8(D), 1DFK and 1KK7 (N), 1KWO, 1KQM, 1L2O(D)
Smooth muscle myosin	<i>Gallus gallus</i>	1BR1(T), 1BR2(T), 1BR4(T)
Myosin II S1	<i>Gallus gallus</i>	2MYS(N)
Myosin V	<i>Gallus gallus</i>	1OE9(R)
MyoE (class I)	<i>Dictyostelium discoideum</i>	1LXX(T)

Myosin states are *T*, transition; *N*, near-rigor; *R*, rigorlike; and *D*, detached. We only keep kinesin/myosin structures with complete coordinates for all residues in the nucleotide-pocket.

structures (27 in total). The goal is twofold: first to identify the dominant conformational changes among them, and second, to cluster those pocket conformations (see Materials and Methods). The PCA is performed with reference to a transition state structure (PDB: 1VOM).

The observed structural changes of the nucleotide-pocket are dominated by the top two principal components P_1 and P_2 which are used to cluster those conformations in a two-dimensional plot: each pocket conformation is represented by two projection coefficients obtained by projecting the conformational changes from the reference structure onto P_1 and P_2 (see Materials and Methods). Not surprisingly, they fall into two main clusters corresponding to the transition state and the near-rigor/detached state, and two outliers (PDB: 1Q5G and 1OE9) belonging to the rigorlike state (Fig. 1 *a*). This is consistent with the classification of structural states (5), and it supports the strong correlation between the nucleotide-pocket conformation and the global conformation of the myosin motor domain, and justifies the validity of

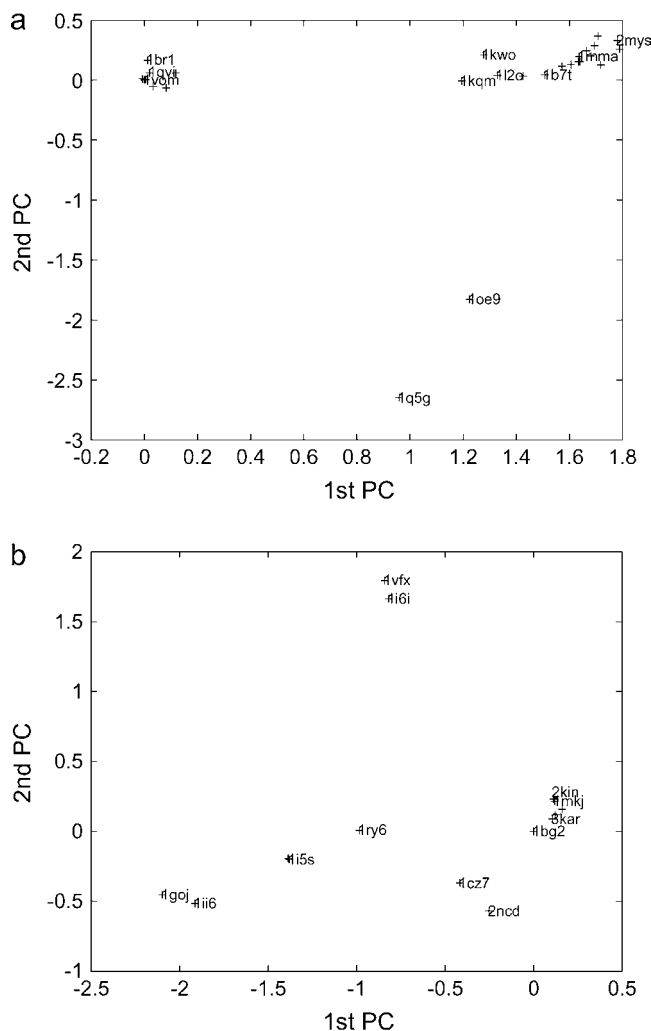


FIGURE 1 Two-dimensional clustering of the nucleotide-pocket conformations for (a) myosins with reference to 1VOM; and (b) kinesins with reference to 1BG2 by using the top two components obtained from PCA. For myosins, three clusters are found: cluster 1 (1VOM, 1MND, 1DFL, 1QVI, 1LXX, 1BR1, 1BR2, 1BR4), cluster 2 (1Q5G, 1OE9), and cluster 3 (the remaining structures). For kinesins, one main cluster (1BG2, 1MKJ, 2KIN, 3KAR, 1F9U, 1F9T) is found, whereas the rest are not well-clustered (2NCD, 1CZ7, 1II6, 1GOJ, 1I5S, 1VFX, 1I6I, 1VFX, 1RY6). For clarity, only some of the PDB names are marked in the figure.

studying the pocket dynamics as an indirect means to probe the global dynamics.

The structural changes described by P_1 are dominated by a very large movement of the switch II (Fig. 4 *a*), which is observed when one does structural comparison between the near-rigor state structures and the transition state structures. Historically, the near-rigor state was proposed to be reached at the end of a power stroke on release of MgADP; however, kinetic evidence showed that it cannot bind strongly to actin without significant structural rearrangements (3). Therefore the near-rigor state is probably reached from the strong-binding rigor state instead of the transition state during the working cycle. So a direct transition from transition state to

near-rigor state is probably not relevant to the power-stroke mechanism.

The structural changes described by P_2 simultaneously involve large movements of P loop, switch I and switch II (Fig. 4 *b*). This largely accounts for the transition from the transition state (PDB: 1VOM) to the rigorlike state (PDB: 1Q5G, 1OE9), which involves the opening of both switch I and switch II. As observed by Coureux and co-workers (6): in 1OE9, the P loop and switch I move apart by 6.5 Å (P loop was used for structural alignment so its movement was not reported); a new conformation for switch II is stabilized by new interactions; and switch I conformation follows the movement of the upper 50-kDa subdomain relative to the P loop and the N-terminal subdomain. Similar pocket changes were observed in another rigorlike structure 1Q5G (7): in particular, the opening of switch I and the further opening of switch II in the near-rigor structure (PDB: 1MMA). A transition from the weak-binding transition state to the strong-binding rigor state is believed to be critical to the power-stroke generation (6,7).

Effects of elastic coupling between nucleotide-pocket and its environment

We now examine the effects of the elastic coupling between the nucleotide-pocket and its environment on the local dynamics of the pocket. We compute the root-mean-square fluctuation (RMSF) (see Eq. 6) based on the subsystem NMA of the nucleotide-pocket in the absence and presence of the elastic coupling, respectively (Fig. 2 *a*).

We find that the coupling to the environment significantly suppresses the overall RMSF (especially in that the two major peaks in switch I and N_4 at zero coupling are sharply reduced). In the RMSF plot (Fig. 2 *a*), major peaks are found in switch I (peaked at its N-terminal), switch II (peaked at its C-terminal), and N_4 (peaked at its C-terminal). This suggests that the coupling with the environment significantly affects the local dynamics of the nucleotide-pocket by sharply reducing its fluctuation nonuniformly.

Comparison of the measured RMSD with the computed RMSF in the nucleotide-pocket

For comparison, we structurally align the pocket conformation of every myosin structure with the pocket conformation of a chosen reference structure (PDB: 1VOM), then we plot the RMSD at each residue in the pocket (Fig. 3 *a*). This gives the measured amplitude of conformational changes in the pocket, which can be qualitatively compared with the RMSF to examine if the latter captures the observed structure changes in amplitude: namely, do major peaks in the RMSD match with the peaks in RMSF?

The RMSD plot shows two interesting features: first, large-scale movement in switch II dominates the RMSD for pairs between the transition state and the near-rigor or

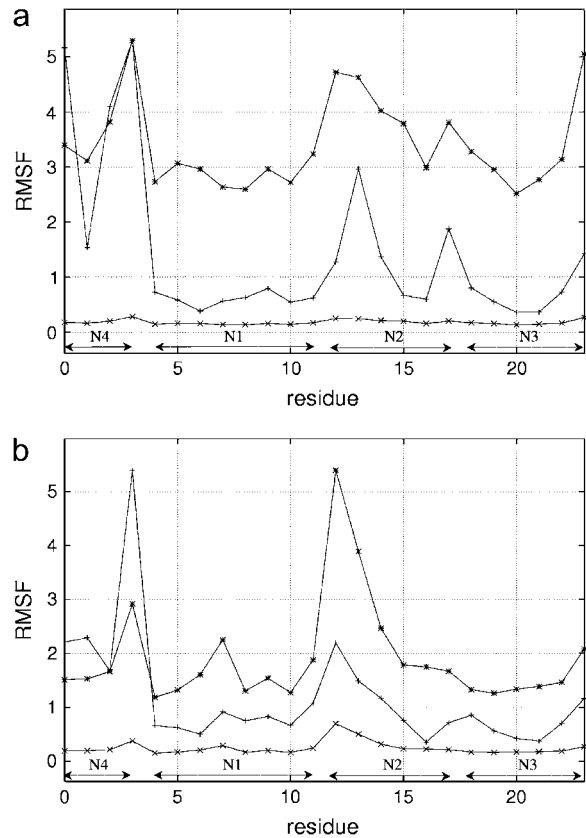


FIGURE 2 Computed RMSF based on the subsystem NMA for (a) 1VOM, (b) 1BG2. The line with plus symbols is the RMSF at zero coupling, the other two are the RMSF in the presence of elastic couplings (*line with x-marks* indicates real-scale; *line with stars* indicates rescaled for clarity). The ranges of the four pieces (N_1 – N_4 , N_2 is switch I; N_3 is switch II) of the nucleotide-pocket are marked.

detached state; second, several large-scale structural changes in switches I, II, and P loop are observed for pairs between the transition state and the rigorlike state. These observations are also consistent with the two principal components P_1 and P_2 obtained by PCA (see above).

The RMSF shows large fluctuation in switches I, II, and N_4 , which is largely consistent with the RMSD results (Fig. 3 *b*): first, the large structural changes in switch I (peaked at its N-terminal) and switch II (peaked at its C-terminal) as shown in the RMSD plot are qualitatively consistent with similar peaks in the RMSF plot; second, the peak in P loop is also seen at its third residue in the RMSF plot, although it is lower than in the RMSD plot; and third, the peak in N_4 appears to be higher in the RMSF plot than in the RMSD plot.

We note that the differences between the RMSD and RMSF (in the P loop and N_4) may be due to the oversimplification of ENM parameterization and the lack of consideration of the interaction with ligand. Despite this limitation, the large fluctuations in both switch I and II are captured by the present analysis, which may be important to the myosin motor function.

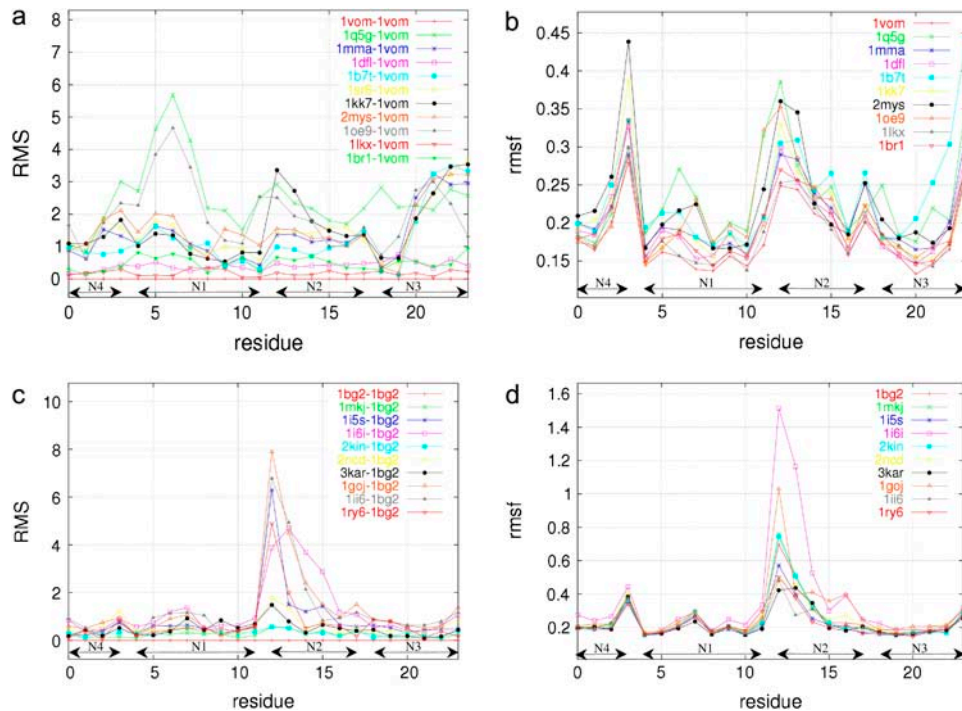


FIGURE 3 Comparison of the measured RMSD with the computed RMSF: (a) RMSD with respect to 1VOM; (b) computed RMSF for myosin nucleotide-pockets; (c) RMSD with respect to 1BG2; and (d) computed RMSF for kinesin nucleotide-pockets. The ranges of the four pieces (N_1 – N_4 , N_2 is switch I; N_3 is switch II) of the nucleotide-pocket are marked.

Comparison of pocket-modes with measured conformational changes

We now examine if individual normal modes can describe the observed conformational changes in the nucleotide-pocket.

We examine all measured conformational changes from the reference pocket structure (PDB: 1VOM), and project them to each pocket-mode solved from the subsystem NMA. Interestingly, we find that the pocket structural changes from the transition state (PDB: 1VOM) to the rigorlike state (PDB: 1Q5G) are dominated by the lowest non-zero mode #1 with overlap 0.58; meanwhile, the pocket conformational changes from 1VOM to the near-rigor state (PDB: 1MMA) are not dominated by any single mode (the highest overlap is with mode #6: 0.39).

Similarly, we can also compare the normal modes with the two principal components P_1 and P_2 obtained from PCA (see above). We find similar results: P_2 overlaps significantly with mode #1 (overlap = 0.66, see Fig. 4 b), whereas P_1 is not dominated by any single mode (the highest overlap is with mode #6: 0.41, see Fig. 4 a).

A comparison between P_2 and mode #1 indicates (Fig. 4 b): mode #1 involves large-scale movement in switches I, II, and N_4 (Fig. 5 b) and it gives a good description of the switch I and switch II movement in P_2 , although the N_4 movement is overestimated and the P loop movement is underestimated.

In summary, the observed pocket structural changes described by P_2 are better accounted for by a single mode than the one described by P_1 , especially in switch I and II. This suggests that a coordinated movement of both switches

with comparable amplitude is dynamically prone to occur (involving mainly a single mode) with a low-energy barrier, whereas the movement by switch II alone (as described by P_1) is dynamically more complex (involving multiple modes) and energetically less favorable.

Global conformational changes beyond the nucleotide-pocket

In response to the pocket deformation described by the relevant mode #1, the subdomains (environment) around the pocket will move accordingly to relax the strain caused by the pocket structural changes. We can calculate the global conformational changes induced by the pocket deformation (see Materials and Methods), and project it to the low-frequency global modes to identify the modes of global motions induced by the pocket deformation.

We find the dominant non-zero mode to be mode #7 (overlap = 0.49 if excluding six zero-modes), which was recently identified as the dominant mode in the dynamical correlations among three functionally critical regions (the cleft between the upper and lower 50-kDa subdomains, the nucleotide-binding pocket and the converter) (21): it involves simultaneous hinge motions of the opening/closing of the 50-kDa cleft and the swinging motion of the converter, and the nucleotide-pocket lies at its hinge region (Fig. 5 a).

Therefore, the relevant pocket-mode involved in the local dynamics (#1) is consistent with the relevant global mode involved in the global dynamics (#7), in that the former can effectively trigger the latter via elastic couplings in the

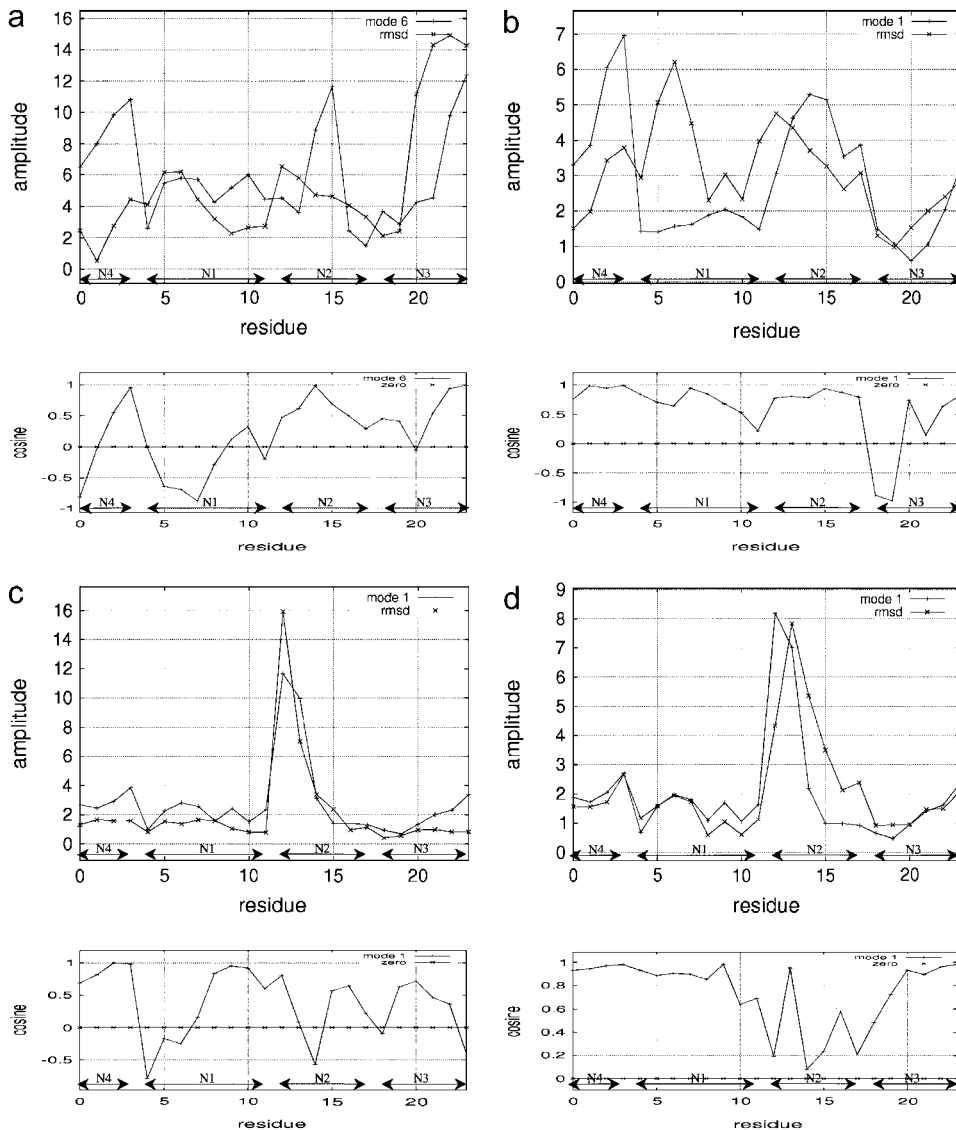


FIGURE 4 Comparison of the top two principal components with the eigenvector of the dominant pocket-mode. (a) First principal component of myosin pockets, and (b) second principal component of myosin pockets. (c) First principal component of kinesin pockets, and (d) second principal component of kinesin pockets. Top panel compares the amplitude, whereas the bottom panel plots the cosine of the angle between them. The ranges of the four pieces (N_1 – N_4 , N_2 is switch I; N_3 is switch II) of the nucleotide-pocket are marked.

framework of ENM. This strongly supports the existence of a dynamical pathway that transmits the small deformation at the nucleotide-pocket to the remote sites of the myosin motor to ultimately trigger global motions that modulate the actin-binding and cause motor movement. This pathway is clearly revealed by the present analysis where the elastic coupling plays a key role in mediating the connection between the local dynamics of the nucleotide-pocket and the global dynamics of the whole motor.

Kinesin's nucleotide-pocket dynamics

Comparison of nucleotide-pocket conformations between kinesins and myosins

Although myosins and kinesins have a highly homologous nucleotide-binding pocket, they differ significantly in pocket conformation as revealed by crystallographic studies.

All kinesins show a tightly closed pocket in the ADP state (as defined by P loop-switch II distance; see Ref. 10), comparable with myosins in the ATP state (transition state). In contrast, switch I in kinesins is essentially open, although it is closed in all except the rigorlike state in myosins (8). Evidence from electron paramagnetic resonance shows that switch I closes when kinesin binds to microtubules (27), which is opposite to the observation that switch I opens when myosin binds to actin (6–9).

The extent of openness in switch I differs quantitatively among different kinesin structures. As proposed by Song and co-workers (28), the distance from the conserved *N* of switch I to the conserved *G* of P loop is used to assess the pocket openness. In PDB structure 1GOJ, those two residues (G88 and N202) are 22.7 Å apart, making the nucleotide-binding pocket very widely open, consistent with the largest RMSD at the N-terminal end of switch I observed for pair 1GOJ-

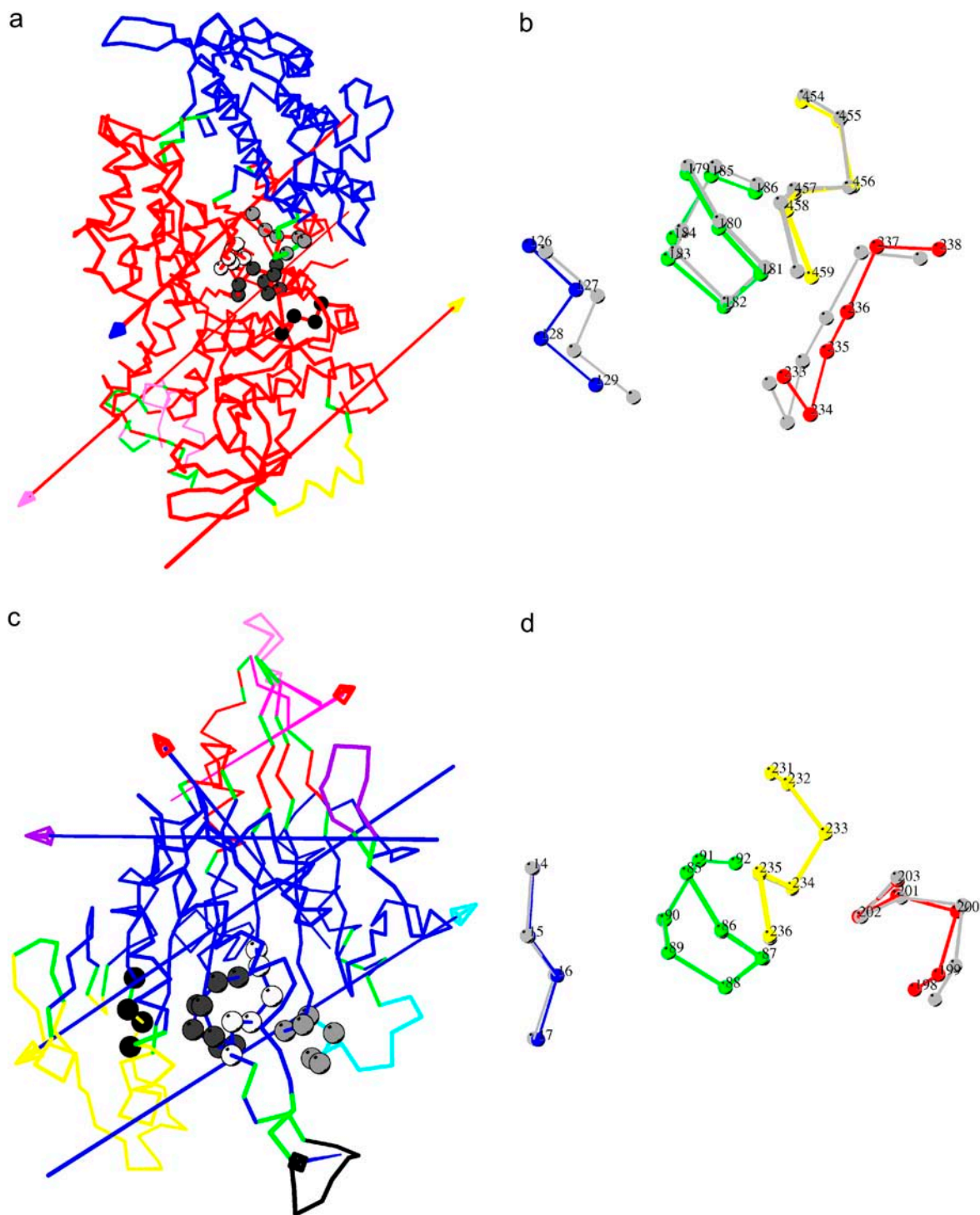


FIGURE 5 Dynamical domains partition for the global modes triggered by the pocket deformation described by the relevant pocket-mode. (a) Global mode #7 of 1VOM describes the following hinge motions: Opening/closing of the upper 50-kDa subdomain (blue) versus the lower 50-kDa subdomain (red), flipping of a part of N-terminal subdomain (yellow), rotation of converter (violet). (b) The nucleotide-pocket conformational changes described by the pocket-mode #1 of myosin 1VOM. (c) Global mode #10 of 1BG2 describes the following hinge motions: switch I ($\alpha 3$ -L9- $\alpha 3a$: cyan) flipping, L11 loop (black) flipping, flipping of the region $\beta 5a$ -L8- $\beta 5b$ (purple), tip loops (L6 and L10: violet) flipping and the twisting motion of the compact subdomain including helix H6 (yellow). (d) The nucleotide-pocket conformational changes described by the pocket-mode #1 of kinesin 1BG2. In *a* and *c*, the nucleotide-pocket residues are shown as solid circles (four levels of grayscale from dark to light, for N4, N1, N2, and N3, respectively). In *b* and *d*, the colors blue, green, red, and yellow are for N4, N1, N2, and N3, respectively, and the gray trace represents the pocket conformation after the displacement. The partition of dynamical domains (distinguished by different colors) is done by DynDom. The hinge/bending regions are colored by green. The rotation axis for each pairwise interdomain motion is shown as an axis with an arrowhead; the color of the axis stem is set to be the same as the domain fixed for the structural alignment, whereas the color of the arrowhead is set to be the color of the moving domain.

1BG2 (Fig. 3 *c*); for PDB structure 2KIN, the corresponding distance (between G86 and N199) is only 15.8 Å. The narrowest pocket is seen in PDB structure 2NCD, where the bulge loop tightens the entrance of the active site further.

The switch I undergoes other large structural changes too (in PDB structure 1I6I, for example). The sharply different conformations of switch I in kinesins from those in myosins may hint for its different functional roles.

Principal components analysis of nucleotide-pocket conformations from crystal structures

Similar to the analysis of myosins, we perform a PCA for all the pocket conformations from the available kinesin structures (15 in total). The PCA is with reference to an ADP state structure (PDB: 1BG2).

The observed structural changes in the nucleotide-pocket are dominated by the top two principal components P_1 and P_2 which are used to cluster the pocket conformations in a two-dimensional plot (Fig. 1 *b*). Unlike myosins, they form one main cluster and the rest are spread out (Fig. 1 *b*). This is consistent with the lack of a clear classification of kinesin structures.

The structural changes described by P_1 are dominated by large switch I movement (peaked at its N-terminal, see Fig. 4 *c*), which largely accounts for the switch I opening observed in, for example, the conformational changes between the pair (1BG2 → 1GOJ).

The structural changes described by P_2 are also dominated by large switch I movement (peaked at its second residue, see Fig. 4 *d*), which mainly accounts for the switch I structural changes observed in the conformational changes between the pair (1BG2 → 1I6I). In 1I6I (an ATP-like structure of KIF1A motor complexed with AMP·PCP; see Ref. 29), switch I assumes a substantially different conformation: a pseudo- β -hairpin rather than a short loop-helix-loop as observed in other kinesin structures.

It is interesting that unlike myosins, both P_1 and P_2 describe large structural changes in switch I whereas the other parts including switch II move much less in amplitude.

Effects of elastic coupling between nucleotide-pocket and its environment

We now compute the RMSF for the nucleotide-pocket in the absence and presence of the elastic couplings, respectively (Fig. 2 *b*). Similar to myosins, the coupling to the environment significantly suppresses the overall RMSF (especially the two major peaks in switch I and N_4 are sharply reduced); one dominant peak is found in switch I (peaked at its N-terminal), with several much lower peaks in the P loop, switch II, and N_4 . Unlike in myosins, the RMSF in switch I is suppressed less significantly in kinesins, so it becomes the dominant peak that is much higher than the others.

Comparison of measured RMSD with computed RMSF in the nucleotide-pocket

The RMSD plot shows that the large-scale structural change in switch I (peaked at its N-terminal) dominates the RMSD for all pairs (Fig. 3 *c*). This is consistent from the two principal components obtained by PCA (see above). The structural comparison study in Sack et al. (10) also identified the switch I loop ($\alpha 3$ – $\alpha 3a$ region) as the largest main-chain deviations, which primarily consist of bending of helix $\alpha 3$ at its C-terminal end (or N-terminal end of switch I loop).

Consistent with the RMSD results, the RMSF also shows a dominantly large fluctuation in switch I (Fig. 3 *d*).

Unlike myosins, where switch I and switch II have comparable RMSF, switch II movement is relatively weak in kinesins. The observation of “closed switch II and open switch I” in kinesins may explain the significantly enhanced/reduced RMSF of switch I/switch II in kinesins as compared with myosins. Since microtubule-binding sites are closer to switch II than switch I, we expect such disparity between them to persist upon binding with microtubules, which probably has a stronger restraining effect on switch II than switch I.

Comparison of pocket-modes with measured conformational changes

We now assess how well the pocket-modes describe the observed conformational changes of the nucleotide-pocket.

We examine all individual conformational changes from the reference pocket structure (PDB: 1BG2), and compare them with the pocket-modes solved from the subsystem NMA. Similar to myosins, we find that these pocket structural changes are dominated by the lowest non-zero mode (#1) with significant overlap (Table 2).

Then we compare the above relevant mode with the two principal components P_1 and P_2 obtained from PCA. Both P_1 and P_2 overlap significantly with mode #1 (Table 2).

TABLE 2 Results of comparing the subsystem normal modes with the measured structural changes in the nucleotide-pocket of myosins (*upper row*) and kinesins (*lower row*)

Pair	Mode:	Overlap
(1Q5G-1VOM)	#1:	0.58
(1MMA-1VOM)	#6:	0.39
(1B7T-1VOM)	#6:	0.47
(1OE9-1VOM)	#1:	0.45
(P_1 -1VOM)	#6:	0.41
(P_2 -1VOM)	#1:	0.66
(1MKJ-1BG2)	#1:	0.80
(1I5S-1BG2)	#1:	0.52
(2NCD-1BG2)	#1:	0.87
(1I6I-1BG2)	#1:	0.58
(1GOJ-1BG2)	#1:	0.54
(P_1 -1BG2)	#1:	0.50
(P_2 -1BG2)	#1:	0.59

A detailed comparison between P_1 , P_2 , and mode #1 indicates: mode #1 involves large-scale movement in switch I (peaked at its N-terminal, see Fig. 5 *d*), and it gives a good description of the switch I movement in both P_1 and P_2 (Fig. 4, *c* and *d*).

To summarize, the observed pocket structural changes are well described by a single mode, which is dominated by a large movement in switch I, suggesting that a large structural change of switch I alone is dynamically prone to occur with a low-energy barrier, whereas the large movement by switch II is less favorable.

The dominantly large movement of switch I in kinesins, as contrary to myosins, is consistent with its exposure at the surface of the kinesin motor (in myosins, it is buried by the upper 50-kDa and N-terminal subdomains). Furthermore, this movement may be functionally important. Evidence from electron paramagnetic resonance shows that switch I closes when kinesin binds to microtubules (27). Another study, by Yun et al. (11), also suggested that the inward movement of switch I may accelerate ADP release and thus serve as the end-link of a pathway extending from microtubule-binding $\alpha 4$ helix to switch I that modulates the microtubule-binding-activated ATPase cycle. Although the binding of the microtubules may restrain the large fluctuation of switch I, because switch I does not appear to directly bind to microtubules, its restraining effect is probably not as drastic as the upper 50-kDa subdomain in myosins. Therefore, the dominantly high mobility/flexibility of switch I may be a functionally relevant feature that distinguishes kinesins from myosins in their force-generation mechanism, rather than an artifact due to the lack of binding of microtubules. Meanwhile, although in kinesins, switch II has much weaker fluctuation than switch I, it can still play some critical functional roles, such as sensing the binding of microtubules that would cause large structural changes to its neighboring L11 loop and $\alpha 4$ helix. Therefore, it is likely that both switches coordinate dynamically in different manners to fulfill their function in kinesin and myosins.

Global conformational changes beyond the nucleotide-pocket

Finally we compute the global conformational changes induced by the pocket deformation described by the relevant mode #1 as identified above.

We find that the induced global structural changes are dominated by mode #10 (overlap = 0.48 if excluding six zero-modes). Unlike the other low-frequency global modes describing local movements, this mode is highly collective and it simultaneously involves multiple bending/twisting motions as follows (Fig. 5 *c*): bending motions of region $\beta 5a$ -L8- $\beta 5b$, switch I region, L11 loop and the tip of the motor arrowhead (L6 and L10); and the twisting motion of the compact subdomain including H6 helix. It is interesting that this single mode spans a pathway of hinge regions

connecting switch I, switch II with H6 helix which is connected to the neck-linker, and it also involves the bending motions of two putative microtubule-binding regions: $\beta 5a$ -L8- $\beta 5b$ and L11 (see Ref. 10 for naming scheme of secondary structure segments of kinesins). This suggests a possible dynamical pathway via which the pocket deformation can trigger global structural changes that modulate the microtubule-binding sites and the neck-linker. In particular, the twisting motion may change the orientation of the H6 helix and thereby modulates the docking/undocking of the neck-linker. It is interesting that this pathway appears to be relayed via N_4 instead of the $\alpha 4$ helix from the nucleotide-pocket to the neck-linker.

We note that the $\alpha 4$ -L12- $\alpha 5$ region (another putative microtubule-binding site) and the C-terminal half of H6 helix are not involved in the global structural changes described by mode #10. Indeed, it appears that these regions are dynamically frozen (with reduced fluctuation) in ENM (18) which seems to be at odds with crystallographic data that shows $\alpha 4$ helix can move as a separate domain, effectively sliding over the back side of the central β -sheet (10). It is likely that the elastic interactions with uniform force constant do not correctly describe the physical interactions around the $\alpha 4$ helix. So the above results should be viewed as complimentary to, rather than against, alternative pathways from/to the nucleotide-pocket that pass the $\alpha 4$ -L12- $\alpha 5$ region (11).

Justification of flexible environment and elastic interactions

For myosins, the treatment of the surrounding subdomains as flexible and mobile objects that can respond to the pocket changes seems to be supported by the observation of the following conformational changes: In the PDB structure 1OE9, switch I follows the rotation of the upper 50-kDa subdomain relative to the P loop and the N-terminal subdomain. Accompanied with the pocket changes, a distortion of the seven-stranded β -sheet that couples the N-terminal subdomain and the upper 50-kDa subdomain appear to be essential to allow large movement of the upper 50-kDa subdomain and switch I and switch II to follow it (6). The elastic-interactions-based description of myosin motor domain is supported by our recent work (18,21), which showed that the ENM indeed gives a good description of the observed conformational changes and the inter-subdomains' dynamical correlations.

Similarly, for kinesins, for there to be a dynamical pathway that connects the nucleotide-pocket with remote regions of the motor domain, it seems reasonable to treat the environment around the pocket as flexible and fluctuating, rather than as rigid and fixed objects. However, whether elastic interactions (instead of irreversible and nonharmonic interactions) are able to explain the signal transmission in a single-domain globular protein like kinesin is still controversial. The results of the present study are quite

encouraging in clarifying this controversy: although the ENM with uniform force constant is probably not accurate enough to describe the movements of all parts of kinesin motor, it appears to give a quantitatively good description of the structural changes in the nucleotide-pocket, which is consistent with crystallographic data; and it provides at least some qualitative insight into the possible mechanism by which the pocket deformation can be transmitted via the collective global motions it triggers, which may exist in single-domain proteins as well as in multidomain proteins. After all, single-domain proteins with knobs on them (like kinesins) are not so different dynamically from multidomain proteins (like myosins), and both can utilize collective motions to mediate long-range signal transmissions.

Relations to functional mechanisms of myosins and kinesins

For myosins, the above results clearly show that the relevant nucleotide-pocket dynamics (characterized by the pocket-mode #1) is elastically coupled with the relevant global dynamics (described by the global mode #7), which is consistent with the widely-hypothesized pathways connecting pocket deformations with actin-binding and force generation via several key joints (5).

For kinesins, the picture is more elusive for the lack of crystal structures for the strong-binding state. Indeed, it is difficult to identify a handful of relevant global modes simply by a structural comparison of the available crystal structures (18). The present study suggests a promising alternative strategy of finding the relevant global modes: we first find the pocket-mode relevant to the nucleotide-pocket dynamics and then use it to induce the global conformational changes (18). This strategy has indeed generated some enlightening results: a collective global mode (#10) is revealed from the induced global structural changes, which describes multiple bending/twisting motions that involve several functional sites. Further study is needed to test the validity of this result.

The above results support the potential power of the ENM-based analysis that is not limited to the description of single hinge motions of multidomain proteins. Instead, a collective mode is able to encode a rather complex pattern of multiple hinge motions that may account for the mechanism of long-range allostery.

Comparison with the analysis based on global modes

Compared with the NMA of the whole protein complex where global modes are solved and analyzed, the subsystem NMA proposed here has the following advantages: first, it is computationally more cost-effective—it reduces the analysis of the complex dynamics of a large biomolecular system to the analysis of a smaller subsystem, with the effects of the coupling with its environment implicitly incorporated.

Second, it is able to selectively probe the low-energy dynamics specific to the chosen subsystem—only the global dynamics coupled with the local dynamics of the given subsystem is probed, which effectively excludes many irrelevant degrees of freedom and significantly simplifies the task of finding the relevant modes (for example, the global modes triggered by the nucleotide-pocket deformation in myosins and kinesins). This is particularly helpful, considering the generally large size of the normal-modes spectrum (three times the number of residues), which poses a tremendous challenge to researchers to make sense of them.

For future work, the analysis of subsystem dynamics introduced in this work will be applied to other protein complexes to address a number of intriguing issues, such as, for example, finding dynamical pathways that transmit signals of ligand binding to remote sites, comparing functional dynamics of homologous enzymes sharing similar active site, etc. We will also work on the refined parameterization of the ENM beyond uniform force constant to quantitatively improve the results.

This work is supported by the National Institutes of Health.

REFERENCES

1. Kull, F. J., and S. A. Endow. 2002. Kinesin: switch I & II and the motor mechanism. *J. Cell Sci.* 115:15–23.
2. Geeves, M. A., and K. C. Holmes. 1999. Structural mechanism of muscle contraction. *Annu. Rev. Biochem.* 68:687–728.
3. Houdusse, A., and H. Sweeney. 2001. Myosin motors: missing structures and hidden springs. *Curr. Opin. Struct. Biol.* 11:182–194.
4. Kull, F. J., E. P. Sablin, R. Lau, R. J. Fletterick, and R. D. Vale. 1996. Crystal structure of the kinesin motor domain reveals a structural similarity to myosin. *Nature.* 380:550–555.
5. Houdusse, A., A. G. Szent-Gyorgyi, and C. Cohen. 2000. Three conformational states of scallop myosin S1. *Proc. Natl. Acad. Sci. USA.* 97:11238–11243.
6. Coureux, P. D., A. L. Wells, J. Menetrey, C. M. Yengo, C. A. Morris, H. L. Sweeney, and A. Houdusse. 2003. A structural state of the myosin V motor without bound nucleotide. *Nature.* 425:419–423.
7. Reubold, T. F., S. Eschenburg, A. Becker, F. J. Kull, and D. J. Manstein. 2003. A structural model for actin-induced nucleotide release in myosin. *Nat. Struct. Biol.* 10:826–830.
8. Holmes, K. C., I. Angert, F. J. Kull, W. Jahn, and R. R. Schroder. 2003. Electron cryo-microscopy shows how strong binding of myosin to actin releases nucleotide. *Nature.* 425:423–427.
9. Volkman, N., D. Hanein, G. Ouyang, K. M. Trybus, D. J. DeRosier, and S. Lowey. 2000. Evidence for cleft closure in actomyosin upon ADP release. *Nat. Struct. Biol.* 7:1147–1155.
10. Sack, S., F. J. Kull, and E. Mandelkow. 1999. Motor proteins of the kinesin family. Structures, variations, and nucleotide binding sites. *Eur. J. Biochem.* 262:1–11.
11. Yun, M., X. Zhang, C. G. Park, H. W. Park, and S. A. Endow. 2001. A structural pathway for activation of the kinesin motor ATPase. *EMBO J.* 20:2611–2618.
12. Wriggers, W., and K. Schulten. 1998. Nucleotide-dependent movements of the kinesin motor domain predicted by simulated annealing. *Biophys. J.* 75:646–661.

13. Minehardt, T. J., R. Cooke, E. Pate, and P. A. Kollman. 2001. Molecular dynamics study of the energetic, mechanistic, and structural implications of a closed phosphate tube in NCD. *Biophys. J.* 80:1151–1168.
14. Vale, R. D., and R. A. Milligan. 2000. The way things move: looking under the hood of molecular motor proteins. *Science*. 288:88–95.
15. Atilgan, A. R., S. R. Durell, R. L. Jernigan, M. C. Demirel, O. Keskin, and I. Bahar. 2001. Anisotropy of fluctuation dynamics of proteins with an elastic network model. *Biophys. J.* 80:505–515.
16. Delarue, M., and Y. H. Sanejouand. 2002. Simplified normal mode analysis of conformational transitions in DNA-dependent polymerases: the elastic network model. *J. Mol. Biol.* 320:1011–1024.
17. Tama, F., and Y. H. Sanejouand. 2001. Conformational change of proteins arising from normal mode calculations. *Protein Eng.* 14:1–6.
18. Zheng, W., and S. Doniach. 2003. A comparative study of motor-protein motions by using a simple elastic-network model. *Proc. Natl. Acad. Sci. USA*. 100:13253–13258.
19. Li, G., and Q. Cui. 2004. Analysis of functional motions in Brownian molecular machines with an efficient block normal mode approach: myosin-II and Ca^{2+} -ATPase. *Biophys. J.* 86:743–763.
20. Navizet, I., R. Lavery, and R. L. Jernigan. 2004. Myosin flexibility: structural domains and collective vibrations. *Proteins*. 54:384–393.
21. Zheng, W., and B. R. Brooks. 2005. Identification of dynamical correlations within the myosin motor domain by the normal mode analysis of an elastic network model. *J. Mol. Biol.* 346:745–759.
22. Tirion, M. M. 1996. Large amplitude elastic motions in proteins from a single-parameter, atomic analysis. *Phys. Rev. Lett.* 77:1905–1908.
23. Hinsen, K. 1998. Analysis of domain motions in large proteins. *Proteins*. 33:417–429.
24. Brooks, B. R., D. Janezic, and M. Karplus. 1995. Harmonic analysis of large systems. *J. Comput. Chem.* 16:1522–1542.
25. Levy, R., A. Srinivasan, W. Olson, and J. McCammon. 1984. Quasiharmonic method for studying very low frequency modes in proteins. *Biopolymers*. 23:1099–1112.
26. Hayward, S., and H. J. Berendsen. 1998. Systematic analysis of domain motions in proteins from conformational change: new results on citrate synthase and T4 lysozyme. *Proteins*. 30:144–154.
27. Naber, N., T. J. Minehardt, S. Rice, X. Chen, J. Grammer, M. Matuska, R. D. Vale, P. A. Kollman, R. Car, R. G. Yount, R. Cooke, and E. Pate. 2003. Closing of the nucleotide pocket of kinesin-family motors upon binding to microtubules. *Science*. 300:798–801.
28. Song, Y. H., A. Marx, J. Muller, G. Woehlke, M. Schliwa, A. Krebs, A. Hoenger, and E. Mandelkow. 2001. Structure of a fast kinesin: implications for ATPase mechanism and interactions with microtubules. *EMBO J.* 20:6213–6225.
29. Kikkawa, M., E. P. Sablin, Y. Okada, H. Yajima, R. J. Fletterick, and N. Hirokawa. 2001. Switch-based mechanism of kinesin motors. *Nature*. 411:439–445.